



1 **Persistent primary organic tar particles during the regional wintertime hazes in**
2 **North China: insights into their aging and optical changes**

3

4 Lei Liu¹, Jian Zhang¹, Yinxiao Zhang¹, Yuanyuan Wang¹, Liang Xu¹, Qi Yuan¹, Dantong Liu¹, Yele
5 Sun², Pingqing Fu³, Zongbo Shi⁴, and Weijun Li^{1,*}

6

7 ¹Department of Atmospheric Sciences, School of Earth Sciences, Zhejiang University, Hangzhou
8 310027, China

9 ²State Key Laboratory of Atmospheric Boundary Layer Physics and Atmospheric Chemistry, Institute
10 of Atmospheric Physics, Chinese Academy of Sciences, Beijing 100029, China

11 ³Institute of Surface-Earth System Science, Tianjin University, Tianjin 300072, China

12 ⁴School of Geography, Earth and Environmental Sciences, University of Birmingham, Birmingham
13 B15 2TT, UK

14

15 **Correspondence to:* Weijun Li (liweijun@zju.edu.cn)



16 **Abstract**

17 Primary organic aerosol (POA) is a major component of PM_{2.5} in the winter polluted air in the
18 North China Plain (NCP), but our understanding on the atmospheric aging process of POA particles
19 and the resulting influences on their optical properties is limited. As part of the Atmospheric Pollution
20 and Human Health in a Chinese Megacity (APHH-Beijing) programme, we collected airborne
21 particles at an urban site (Beijing) and an upwind rural site (Gucheng, Hebei province) in the NCP
22 during 13–27 November 2016 for microscopic analyses. We confirmed that a distinct group of
23 spherical or irregular POA particles with high viscosity, defined as primary organic tar (POT) particles,
24 was emitted from the domestic coal and biomass burning at the rural site and was further transported
25 to the urban site during the regional wintertime hazes. During the heavily polluted period (PM_{2.5} >
26 200 µg m⁻³), more than 60% of the POT particles were thickly coated with secondary inorganic
27 aerosols (named as core-shell POT-SIA particle) through the aging process, suggesting that POT
28 particles can provide surfaces for the heterogeneous reactions of SO₂ and NO_x. As a result, their
29 average particle-to-core ratios at the rural and urban sites in the heavily polluted period increased to
30 1.60 and 1.67, respectively. Interestingly, we found that the aging process did not change the
31 morphology and sizes of the POT cores, indicating that POT particles are quite inert in the atmosphere
32 and can be transported long distances. We using the Mie theory estimated that the light absorption of
33 individual POT particles was enhanced by ~1.39 times in the heavily polluted period at the rural and
34 urban sites due to the lensing effect of secondary inorganic coatings. We highlight that the lensing
35 effect on POT particles should be considered in radiative forcing models and the governments should
36 continue to promote clean energy in rural areas to effectively reduce primary emissions.



37 **1 Introduction**

38 Atmospheric aerosol particles can affect the regional and global energy budget by scattering and
39 absorbing solar radiation, modify the microphysical properties of clouds by acting as cloud
40 condensation nuclei (CCN) and exert adverse effects on human health such as respiratory and
41 cardiovascular diseases (IPCC, 2013; West et al., 2016). With the rapid industrialization and
42 urbanization in past decades, severe air pollution characterized by high concentrations of fine
43 particulate matter (PM_{2.5}) frequently occurs in China, especially the regional hazes in the North China
44 Plain (NCP), which has received wide concerns from the public, governments, and scientists (Sun et
45 al., 2016). Many previous studies have well documented that the synergetic effects from extensive
46 emissions of primary particles and gaseous precursors, efficient secondary aerosol formation, regional
47 transport, and unfavorable meteorological conditions are the main factors contributing to the haze
48 formation in the NCP (Chang et al., 2018; Liu et al., 2016; Zhong et al., 2019). In particular, the long-
49 term measurements have confirmed that the wintertime haze episodes in Beijing are commonly
50 initiated by regional transport of air pollutants from the south parts of NCP (e.g., Hebei and Henan
51 provinces) under weak southerly winds and then evolved through the massive secondary aerosol
52 formation via heterogeneous reactions (Ma et al., 2017; Sun et al., 2014; Zheng et al., 2015).

53 During the regional transport and evolution of haze episodes, complex physical and chemical
54 processes in the atmosphere, such as condensation, coagulation, and heterogeneous reactions, could
55 largely alter the morphology, composition, size, and mixing state of individual particles, which is also
56 known as “particle aging” (Li et al., 2016a). Particle aging could further influence the optical property,
57 health effects, hygroscopicity, and CCN activity of aerosol particles, although different types of
58 particles might have different impacts (Fan et al., 2020; Li et al., 2016b; Riemer et al., 2019). Up to
59 now, most of the studies conducted in the NCP mainly have applied various bulk online and offline
60 aerosol analytical techniques (e.g., online aerosol mass spectrometer (AMS) and offline ion
61 chromatographer (IC)) to explore mass concentrations, possible sources, and formation mechanisms



62 of different aerosol components, such as sulfate, nitrate, and organic aerosols (Chen et al., 2020;
63 Cheng et al., 2016; J. Li et al., 2020; Sun et al., 2016; Wang et al., 2020). However, the knowledge
64 on the aging process of aerosol particles remains limited. Therefore, it is of great importance to
65 document the aging processes of different particles, which can reveal the particle transformation in
66 the atmosphere and better assess the climatic effects of aerosols (Du et al., 2019; Li et al., 2016a).

67 Field observations have shown that carbonaceous aerosols, including organic aerosol (OA) and
68 black carbon (BC), are the dominant component of PM_{2.5} during the heating season in the NCP, which
69 accounts for more than 50% of the total PM_{2.5} mass concentration (Liu et al., 2020; P. Liu et al., 2017;
70 Zhang et al., 2020). Source apportionment results reveal that residential coal and biomass burning in
71 rural areas are the major contributors to the carbonaceous aerosols during the wintertime haze in the
72 NCP (Li et al., 2017). BC is the major light-absorbing aerosol in the atmosphere, which can strongly
73 absorb solar radiation and thus affect the regional and global climate (Bond et al., 2013; D. Liu et al.,
74 2017; Wang et al., 2014). In recent years, a bunch of studies have well documented the aging process
75 of BC particles and revealed that the secondary inorganic and organic aerosol coatings (e.g., sulfate
76 and organics) can significantly enhance the light absorption capacity of the internally mixed BC
77 particles via the “lensing effect” (Chakrabarty and Heinson, 2018; Y. Wang et al., 2017). Recently,
78 light-absorbing organic aerosols, also known as brown carbon (BrC), has been reported to be
79 ubiquitous in the atmosphere in the NCP (Wang et al., 2018; Xie et al., 2019). Many studies have
80 demonstrated that primary OA (POA) emitted from the residential coal and biomass burning is the
81 major source of BrC and the chemical composition and optical properties of BrC in freshly emitted
82 POA, as well as the BrC in the ambient atmosphere, were analyzed in detail using bulk techniques
83 such as mass spectrometry and UV–visible spectrophotometry (M. Li et al., 2019; X. Li et al., 2020;
84 Song et al., 2018; Sun et al., 2017; Yan et al., 2017). However, only a few studies characterized the
85 microscopic information such as the morphology and mixing state of freshly emitted POA particles
86 by transmission electron microscopy (TEM) (L. Liu et al., 2017; Zhang et al., 2018). The abundance



87 and the aging process of POA particles in the atmosphere and the resulting influences on their optical
88 properties remain unknown in the NCP.

89 This study, as part of the Atmospheric Pollution and Human Health in a Chinese Megacity
90 (APHH-Beijing) programme (Shi et al., 2019), aims to explore the atmospheric aging process of POA
91 particles emitted from the residential coal and biomass combustion following the regional transport
92 and evolution of haze episodes. Individual particle samples were collected in urban Beijing and the
93 surrounding rural regions during the winter campaign and then were analyzed by microscopic
94 methods to obtain the morphology, composition, size, and mixing state of different individual particle
95 types. Besides, the bulk analyses of aerosol chemical components were also conducted to help
96 understand the evolution of haze episodes. We found that a distinct group of POA particles emitted
97 from the domestic coal and biomass burning were abundant in winter in the NCP. For the first time,
98 we characterized the aging process of such POA particles based on microscopic analyses and Mie
99 theory was used to further explore the resulting influences on their optical properties.

100 **2 Experimental methods**

101 **2.1 Sampling sites and sample collections**

102 Field observations were carried out simultaneously at the Beijing (BJ) urban site (39°58'27" N,
103 116°22'16" E) and Gucheng (GC) rural site (39°08'58" N, 115°44'00" E) during 13–27 November
104 2016. The locations of two sampling sites in the NCP are displayed in Fig. 1a. The BJ urban site,
105 located on the rooftop of a two-story building (8 m above ground level (a.g.l.)) in the Tower Division
106 of the Institute of Atmospheric Physics, Chinese Academy of Sciences, is between the north 3rd and
107 4th ring road and surrounded by commercial area and residential apartments (Fig. 1b). The GC rural
108 site, located on the rooftop of a three-story building (12 m a.g.l.) at the Gucheng Integrated
109 Ecological–Meteorological Observation and Experimental Station of the Chinese Academy of
110 Meteorological Sciences in Dingxing county, Hebei province, is 120 km to the southwest of the BJ
111 urban site and surrounded by many villages and farmlands (Fig. 1c). The detailed information about



112 the two sampling sites can be found in the introduction paper of the APHH-Beijing programme (Shi
113 et al., 2019). The 24-h backward trajectories of air masses ending at the height of 100 m (a.g.l.) over
114 the Beijing site (Fig. 1) were calculated using the NOAA Air Resources Laboratory's HYbrid Single-
115 Particle Lagrangian Integrated Trajectory (HYSPLIT) model (Stein et al., 2016).

116 At the BJ urban site, the species in non-refractory submicron aerosols (NR-PM_i) including
117 organic matter (OM), SO₄²⁻, NO₃⁻, NH₄⁺, and Cl⁻ were measured by a high-resolution aerosol mass
118 spectrometer (HR-AMS, Aerodyne Inc., USA). At the GC rural site, PM_{2.5} samples were separately
119 collected during the daytime (8:30 am to 8:00 pm) and nighttime (8:30 pm to 8:00 am the next day)
120 onto 90 mm-diameter quartz fiber filters (Pallflex 7204, Pall Corporation, USA) using a medium-
121 volume sampler (TH-150A, Wuhan Tianhong Instruments Co., Ltd., China) at a flow rate of 100 L
122 min⁻¹ for 11.5 h. Field blank samples were collected for approximately 15 min without starting the
123 sampler. The filters were prebaked at 450°C for 6 h before sampling to remove any possible
124 contaminants. All the collected samples were sealed individually in aluminum foil bags and stored in
125 a refrigerator at -20 °C for further analyses.

126 Individual particle samples were collected onto copper (Cu) TEM grids coated by formvar and
127 carbon films (carbon type-B, 300 mesh, Beijing XXBR Technology Co., Ltd., China) at the GC rural
128 and BJ urban sites using an individual particle sampler (DKL-2, Qingdao Genstar Electronic
129 Technology Co., Ltd., China) at a flow rate of 1 L min⁻¹. The DKL-2 sampler consists of a single-
130 stage impactor with a jet nozzle of 0.5 mm in diameter. Sampling duration ranged from 8 s to 3 min
131 depending on the pollution levels to avoid overlap of particles on the TEM grids. Individual particle
132 samples were placed in a clean and airtight container with controlled temperature (T , 25±1°C) and
133 relative humidity (RH, 20±3%) for further analyses. The detailed information about the individual
134 particle samples collected at the two sampling sites is listed in Table S1.

135 Meteorological parameters including T , pressure (P), RH, wind speed (WS), and wind direction
136 (WD) were recorded every 5 min at two sampling sites using a pocket weather station (Kestrel 5500,



137 Nielsen-Kellermann Inc., USA). The hourly concentrations of PM_{2.5} and gaseous pollutants (i.e., SO₂,
138 NO₂, CO, and O₃) during the sampling period at two monitoring stations (i.e., Dingxing government
139 station: 39°15'42" N, 115°48'06" E; Beijing Olympic center station: 40°00'11" N, 116°24'25" E) close
140 to GC rural and BJ urban sites were downloaded from the website of air quality online monitoring
141 and analysis platform (<https://www.aqistudy.cn/>). All the data in this study are presented at the Beijing
142 local time (UTC+8).

143 **2.2 PM_{2.5} chemical analysis**

144 PM_{2.5} samples collected at the GC rural site were analyzed to obtain their water-soluble inorganic
145 ions (WSII), organic carbon (OC), and elemental carbon (EC). For the analysis of WSII, two punches
146 with a diameter of 16 mm from each PM_{2.5} sample were put into a vial, followed by adding 20 mL
147 deionized water (18.2 MΩ). Then these vials were placed in an ultrasonic water bath for 30 min to
148 extract WSII. The solutions were further filtered using PTFE syringe filters with 0.45 μm pore sizes
149 to remove insoluble components and then analyzed by an ion chromatography system (Dionex ICS
150 600, ThermoFisher Scientific, USA). Finally, the concentrations of three anions (Cl⁻, SO₄²⁻, and NO₃⁻)
151 and five cations (Na⁺, NH₄⁺, K⁺, Mg²⁺, and Ca²⁺) were obtained. The concentrations of OC and EC
152 in PM_{2.5} samples were determined by analyzing a 1×1.5 cm² punch from each filter with an OCEC
153 analyzer (Model 5L, Sunset Laboratory Inc. USA), which adopted the NIOSH870 temperature
154 protocol with thermal–optical transmittance for charring correction. The OM concentration was
155 estimated via multiplying OC concentration by a factor of 1.6, based on the previous studies (Xing et
156 al., 2013; Zheng et al., 2015).

157 **2.3 AMS data analysis**

158 The HR-AMS V mode data were analyzed using standard data analysis software (PIKA V1.56D).
159 A constant collection efficiency (CE) of 0.5, similar to the previous studies conducted in winter at the
160 BJ site (Sun et al., 2014), was applied to the HR-AMS datasets to obtain the mass concentrations of
161 NR-PM₁ species. The relative ionization efficiencies used for OM, SO₄²⁻, NO₃⁻, NH₄⁺, and Cl⁻ were



162 1.4, 1.2, 1.1, 5.0, and 1.3, respectively. Positive matrix factorization (PMF) is a receptor model that
163 can identify potential sources without local source profiles provided (Xu et al., 2020). PMF was
164 performed on the high-resolution mass spectra of organics measured by HR-AMS. Six OA factors
165 were identified including fossil fuel-related OA (FFOA), cooking OA (COA), biomass burning OA
166 (BBOA), oxidized primary OA (OPOA), oxygenated OA (OOA), and aqueous-phase OOA (aqOOA).
167 Detailed information on the processing of HR-AMS data during the same campaign can be found in
168 the related paper (Xu et al., 2019).

169 **2.4 Individual particle analysis**

170 Individual particle samples were analyzed using TEM (JEM-2100, JEOL Ltd., Japan) operated
171 at a 200 kV accelerating voltage to acquire the morphology and size of individual particles and mixing
172 state (i.e., internally or externally mixed) of different aerosol components within one individual
173 particle. TEM is equipped with an energy-dispersive X-ray spectrometer (EDS, INCA X-Max^N 80T,
174 Oxford Instruments, UK) to semi-quantitatively detect the elemental composition of individual
175 particles with atomic number greater than six ($Z \geq 6$). It should be noted that Cu peaks in the EDS
176 spectra are not considered due to the interference from the Cu substrate of TEM grids. The distribution
177 of aerosol particles on TEM grids is not uniform, with particle size decreasing from the center to the
178 edge of the distribution area. Therefore, to ensure the analyzed particles are representative, five grids
179 from the center to the edge of the particle distribution area in each sample were selected to conduct
180 TEM analysis. TEM images were manually processed by the RADIUS 2.0 software (EMSIS GmbH,
181 Germany) to determine the particle types, areas, perimeters, and equivalent circle diameters (ECD).
182 After a labor-intensive operation, a total of 1197 particles at the BJ urban site and 2443 particles at
183 the GC rural site were analyzed.

184 Scanning electron microscope (SEM, Ultra 55, Carl Zeiss Microscopy GmbH, Germany) was
185 operated at the 10 kV accelerating voltage and secondary electron (SE2) mode to observe the particle
186 surface topography. Furthermore, particles were imaged at a tilt angle of 75° to realize the



187 visualization of their morphology in the vertical dimension.

188 **2.5 Optical property calculation**

189 Mie theory has been widely used to calculate the optical properties of individual particles
190 (Chylek et al., 2019; Wu et al., 2018; Yu et al., 2019). In this study, the light absorption cross sections
191 (ACS) of the primary organic tar (POT, defined in Section 3.2) particles, as well as the coated POT
192 particles with secondary inorganic aerosol (SIA) shell (named as core-shell POT-SIA particle), at
193 the wavelength of 550 nm were calculated with BHCOAT Mie code (Bohren and Huffman, 1983).
194 Details for the classification of POT and POT-SIA particles, please refer to Section 3.2. For the core-
195 shell POT-SIA particles, a refractive index (RI) of $1.55-0i$ for non-light-absorbing SIA coating
196 (Denjean et al., 2014) and $1.67-0.27i$ for light-absorbing POT core (Alexander et al., 2008) were
197 adopted at the wavelength of 550 nm. The ECD of each POT-SIA particle and its POT core obtained
198 from the TEM images were used respectively as the input particle diameter (D_p) and core diameter
199 (D_c) in the Mie model, which made the calculation sufficient to approximate reality. For the POT
200 particles (including bare POT particles and POT cores), the ECD of each POT particle and one-tenth
201 of it were input as the D_p and D_c , respectively. Then by vanishing the refractive index difference
202 between the shell and core (i.e., POT shell and POT core, $RI=1.6-0.27i$), in which case we can obtain
203 the ACS of POT particles. In addition to the calculations for real individual particles observed from
204 the TEM images, we also constructed the model core-shell POT-SIA particle with different POT
205 core diameters (i.e., $D_c=100, 200, 300, 400, 500, 800, 1300, \text{ and } 1500$ nm) and particle-to-core ratios
206 (i.e., D_p/D_c ranged from 1 to 6 with an interval of 0.1), and calculated their ACS to explore the effects
207 of D_c and D_p/D_c changes on the light absorption enhancement factors (E_{abs}) of POT particles.

208 **3 Results and Discussion**

209 **3.1 Overview of a regional haze episode**

210 A typical regional heavy haze episode in the NCP was observed at the GC rural and BJ urban



211 sites during 22–27 November 2016. Fig. 2 shows time series of PM_{2.5}, aerosol chemical species, and
212 gaseous pollutants (i.e., CO, SO₂, O₃, and NO₂) at two sampling sites during the haze episode. Based
213 on the variations of hourly PM_{2.5} concentrations, three pollution levels are defined: clean (PM_{2.5} ≤ 75
214 μg m⁻³), moderate pollution (75 μg m⁻³ < PM_{2.5} ≤ 200 μg m⁻³), and heavy pollution (PM_{2.5} > 200 μg
215 m⁻³). We classified clean period (21 Nov. 00:00 to 22 Nov. 19:00) and heavily polluted period (22
216 Nov. 20:00 to 27 Nov. 10:00) at the GC rural site; clean period (21 Nov. 00:00 to 24 Nov. 09:00),
217 moderately polluted period (24 Nov. 10:00 to 25 Nov. 16:00), and heavily polluted period (25 Nov.
218 17:00 to 27 Nov. 02:00) at the BJ urban site (Fig. 2). Furthermore, we divided the heavily polluted
219 period at the GC rural site into the early stage (22 Nov. 20:00 to 23 Nov. 20:00), middle stage (23
220 Nov. 20:00 to 24 Nov. 20:00), and late stage (24 Nov. 20:00 to 27 Nov. 08:00), based on the evolution
221 of chemical components in PM_{2.5} (Fig. 2a). The averaged meteorological parameters and mass
222 concentrations of PM_{2.5}, aerosol chemical species, OA factors, and gaseous pollutants in different
223 periods at two sampling sites are summarized in Table S2.

224 The strong northwesterly winds (> 4 m s⁻¹) accompanied with rain and snow invaded the NCP
225 during 20–21 November (Fig. S1), leading to the fast dispersion of air pollutants (Fig. 2). The low *T*
226 (−8 to 5°C) and WS (< 2 m s⁻¹) were displayed after the cold front (Fig. S1), which can facilitate the
227 accumulation of air pollutants (Zhong et al., 2019). At the GC rural site, PM_{2.5} concentration began
228 to increase at 18:00 on 22 November and quickly reached a peak of 394 μg m⁻³ within six hours (Fig.
229 2a). PM_{2.5} chemical analysis reveals that OM (252.8 μg m⁻³) accounted for 83% of the PM_{2.5} at the
230 nighttime of 22 November (Fig. S2a), causing the fast transition from the clean to heavily polluted
231 period directly (Fig. 2a). In the early stage of heavily polluted period, the average PM_{2.5} concentration
232 (288.3 μg m⁻³) increased by a factor of seven compared with that (39.8 μg m⁻³) in the clean period,
233 with OM being the largest contributor (185.1 μg m⁻³) followed by SIA (i.e., sum of SO₄²⁻, NO₃⁻, and
234 NH₄⁺; 36.4 μg m⁻³) (Table S2). At the BJ urban site, the air quality remained clean before 24
235 November under continuous northerly winds (Figs. 2b and S1b). With prevailing winds changing



236 from northerly to southerly on 24 November (Fig. S1b), polluted air parcels in the south of NCP was
237 transported to Beijing (Fig. 1a), which has also been confirmed by another study conducted in the
238 same APHH-Beijing winter campaign (Du et al., 2019). Thus, the concentrations of PM_{2.5}, chemical
239 species in NR-PM₁, CO, and SO₂ at the BJ urban site increased simultaneously and sharply from
240 09:00 on 24 November, causing the transition from the clean period to the moderately polluted period
241 (Fig. 2b). The average PM_{2.5} concentration in the moderately polluted period was 111.0 μg m⁻³, 10
242 times higher than that (10.8 μg m⁻³) in the clean period, and the OM and SIA contributed equally in
243 NR-PM₁ with their average concentrations being 44.4 and 43.4 μg m⁻³, respectively (Table S2).
244 Following the haze evolution, the PM_{2.5} levels increased gradually to 312.3 and 396.8 μg m⁻³ in the
245 middle and late stages of heavily polluted period at the GC rural site and to 281.0 μg m⁻³ in the
246 heavily polluted period at the BJ urban site (Fig. 2 and Table S2). Contrasting to the transition periods
247 at two sampling sites, we found that the SIA concentration increased significantly, meanwhile, the
248 OM concentration only slightly increased at the GC rural and BJ urban sites with the consistent
249 decreasing WS and increasing RH (Figs.2 and S2, Table S2). In a word, we observed that the SIA
250 fraction in fine particles increased and OM fraction decreased following the haze evolution (Fig. S2).

251 Figure S2a shows higher fractions of OM, EC, and Cl⁻ at nighttime than daytime during the
252 whole haze episode at the GC rural site, suggesting the continuous strong local combustion emissions
253 at nighttime. Furthermore, the concentration of Cl⁻ (8–22 μg m⁻³) was much higher than that of K⁺
254 (1–3 μg m⁻³) (Fig. 2a), which suggests more contributions from coal combustion than biomass
255 burning at the GC rural site (Sun et al., 2014; Zhang et al., 2020). Based on the field investigation
256 and PM_{2.5} analysis, we concluded that the explosive increase of PM_{2.5} at the GC rural site was initiated
257 by the strong local emissions and accumulation of POA from residential coal combustion for heating
258 and a small fraction of biomass burning for cooking in rural areas. The PMF analysis shows that the
259 FFOA and BBOA (14.6–30.6 μg m⁻³) contributed significantly (> 30%) to OM in the polluted period
260 at the BJ urban site (Fig. S3 and Table S2), suggesting that POA emitted in rural areas were



261 transported to Beijing under the southerly winds. In summary, the bulk analyses show that POA from
262 residential coal and biomass burning consistently contributed to the regional haze, and SIA produced
263 from the secondary formation had an increasing contribution at higher RH following the haze
264 evolution.

265 **3.2 Classification of individual particle types**

266 In this study, TEM observations show a distinct group of spherical and irregular primary organic
267 particles comprised of C, O, and Si elements during this haze episode (Fig. 3a). These particles are
268 stable under strong electron beams and appear as dark features in TEM images, which reflects their
269 high thickness and refractory properties (Ebert et al., 2016; Liu et al., 2018). The SEM image acquired
270 at a 75° tilt angle shows that these particles did not deform upon impact and retained high vertical
271 dimensions (Fig. 4), indicating that these particles are in a solid state with high viscosity (Reid et al.,
272 2018; Wang et al., 2016). By contrast, the secondary particles (i.e., SIA and organic coating) became
273 flat on the substrate (Fig. 4). Previous studies only defined solid spherical tar balls emitted from coal
274 and biomass burning which are identified as light-absorbing POA (Adachi et al., 2019; C. Li et al.,
275 2019; Pósfai et al., 2003; Zhang et al., 2018). In this study, we observed abundant similar spherical
276 and some additional irregular POA particles sourced from coal and biomass burning in this haze
277 episode. To better represent the morphology and sources of these POA particles, we named them as
278 primary organic tar (POT) particles hereafter (Fig. 3a).

279 Besides, the typical individual particle types, such as SIA (Fig. 3b), mineral (Fig. 3c), soot (Fig.
280 3d), and fly ash/metal (Fig. 3e) particles were also classified during this haze episode. The detailed
281 classification criteria of these particle types derived from the TEM images and their sources can be
282 found in our previous paper (Li et al., 2016a). It should be noted that some SIA particles were coated
283 with secondary organic coatings (Fig. 3b) which were produced from the chemical oxidation of
284 volatile organic compounds (Li et al., 2016b). TEM observations further show the internal mixture of
285 POT or soot particles with SIA, i.e., POT–SIA (Fig. 3f) and soot–SIA (Fig. 3g). To better understand



286 the number variations of different particle types, we further classified the POT and POT–SIA particles
287 as the POT-containing particles, and soot and soot–SIA particles as soot-containing particles.

288 3.3 Relative abundance of individual particle types

289 Figure 5 shows number fractions of different particle types in different periods at GC rural and
290 BJ urban sites. At the GC rural site, POT-containing and soot-containing particles were the major
291 particle types with their corresponding contributions being 37.6% and 35.9% by number, followed
292 by SIA particles (22.4%) in the clean period. When the haze episode occurred at the GC rural site,
293 POT-containing particles became dominant in the early stage of heavily polluted period and its
294 number fraction (64.8%) was nearly twice that (37.6%) in the clean period (Fig. 5a). This result
295 consists well with the bulk $PM_{2.5}$ analysis that shows a sharp increase in OM concentration in the
296 early stage of heavily polluted period (Fig. 2a). With the increasing pollution level from the early
297 stage to the late stage of heavily polluted period, the fraction of POT-containing particles slightly
298 decreased from 64.8% to 50.8%, by contrast, the fraction of SIA particles increased from 4.6% to
299 12.4% (Fig. 5a). The variations of POT-containing and SIA particles are similar to the results from
300 the bulk $PM_{2.5}$ analysis shown in Fig. 2a.

301 At the BJ urban site, the contribution of POT-containing particles (15.1%) in the clean period
302 was much lower than that (37.6%) at the GC rural site (Fig. 5). Following the transition from the
303 clean period to the moderately polluted period at the BJ urban site, the fraction of POT-containing
304 particles (66.2%) increased significantly by more than a factor of four compared with that (15.1%) in
305 the clean period. Meanwhile, the fractions of soot-containing, mineral, and SIA particles decreased
306 largely. When the pollution level changed to the heavily polluted period, similar to the situation at the
307 GC rural site, the fraction of SIA particles increased from 7.8% to 13.2% and the fraction of POT-
308 containing particles decreased slightly from 66.2% to 52.8% (Fig. 5b). Overall, the results from the
309 individual particle analysis consist well with the changes in aerosol chemical components obtained
310 by the bulk analysis as shown in Fig. 2. Furthermore, individual particle analysis reveals that the POT-



311 containing particles dominated ($> 50\%$ by number) in the rural and urban air during the regional
312 wintertime haze episode.

313 **3.4 Atmospheric aging of POT particles following the haze evolution**

314 The TEM images clearly show the morphology and mixing state of individual particles in
315 different polluted periods at GC rural and BJ urban sites (Fig. 6). At the GC rural site, TEM
316 observations reveal abundant bare POT particles in the early stage of heavily polluted period (Fig.
317 6a). These POT particles have been proved to be emitted from the residential coal and biomass
318 burning in the wintertime of northern China in our previous studies (Chen et al., 2017; Zhang et al.,
319 2018). Based on the integrated analyses of individual particles and bulk samples, we confirmed that
320 large amounts of POT particles emitted from the intense domestic coal and biomass burning for
321 heating and cooking significantly contributed to the deterioration of the air quality in rural areas.
322 When the haze episode evolved into the late stage of heavily polluted period, we found that most of
323 the POT particles were coated with SIA (i.e., POT–SIA particle) forming the core–shell structure (Fig.
324 6b). Large amounts of POT particles in the regional haze layer provided surfaces for the
325 heterogeneous reactions of SO_2 and NO_x , which promotes the formation of SIA on POT particles in
326 the humid polluted air (Ebert et al., 2016; Zhang et al., 2017).

327 Following the regional transport of polluted air masses from the south to the north of the NCP,
328 abundant POT particles also occurred in the moderately polluted period at the BJ urban site (Fig. 6c).
329 Therefore, we conclude that the POT particles emitted in the rural areas in the south of the NCP could
330 be transported to the BJ urban site and significantly affect the air quality. Following the haze evolution,
331 similar to those at the GC rural site, the POT particles aged and became core–shell POT–SIA particles
332 at the BJ urban site in the heavily polluted period (Fig. 6d).

333 Based on the mixing state of POT-containing particles, we found that following evolution of the
334 haze episode, the fraction of bare POT particles was reduced by twice from 91.4% in the early stage
335 to 39.6% in the late stage of heavily polluted period at the GC rural site, and the fraction of POT–SIA



336 particles correspondingly increased by seven times from 8.6% to 60.4% (pie charts in Fig. 7).
337 Similarly, at the BJ urban site, the fraction of bare POT particles decreased from 70.4% in the
338 moderately polluted period to 31.4% in the heavily polluted period, and the fraction of POT–SIA
339 particles increased correspondingly from 29.6% to 68.6% (pie charts in Fig. 7). Consequently, the
340 average size of POT-containing particles changed from 505 nm in the early stage to 837 nm in the
341 late stage of heavily polluted period at the GC rural site and from 443 nm in the moderately polluted
342 period to 732 nm in the heavily polluted period at the BJ urban site (Fig. 7a). Interestingly, the average
343 sizes of POT particles (including POT cores and bare POT particles) remained similar following the
344 haze evolution, with respective values being 469, 508, and 465 nm in the early, middle, and late stages
345 of heavily polluted period at the GC rural site and 381 and 379 nm in the moderately and heavily
346 polluted periods at the BJ urban site (Fig. 7b). The average sizes of POT particles at the BJ urban site
347 were slightly smaller than those at the GC rural site, which is reasonable because the POT particles
348 collected at the GC rural site were close to the emission sources and larger particles are more likely
349 to be removed during the regional transport (Seinfeld and Pandis, 2006). Adachi et al. (2018) reported
350 that tar balls retained their spherical shapes and the particle masses and sizes did not change largely
351 when heated to 300°C in TEM. As a result, we conclude that the POT particles should be quite
352 physically stable and chemically inert in the atmosphere, which can be transported long distances.

353 The D_p/D_c ratio can be used to indicate the aging degree of POT-containing particles in the
354 atmosphere (Chen et al., 2017; Li et al., 2011). By calculating the D_p/D_c ratio, we realized the
355 quantification of the aging degree of POT-containing particles as shown in Fig. 8. In the early stage
356 of heavily polluted period at the GC rural site, the POT-containing particles were freshly emitted bare
357 POT particles with a fraction of 91.4% (Fig. 7), therefore, the average D_p/D_c ratio was close to one
358 (1.02). Following the haze evolution at the GC rural and BJ urban sites, the average D_p/D_c ratios
359 increased from 1.08 in the middle stage to 1.60 in the late stage of heavily polluted period at the GC
360 rural site, and from 1.11 in the moderately polluted period to 1.67 in the heavily polluted period at



361 the BJ urban site. The results indicate that the POT particles were thickly coated with SIA due to the
362 particle aging process in the haze. Here we can obtain two conclusions based on the individual particle
363 analysis: (1) more POT particles continuously aged and were coated with SIA following the haze
364 evolution; (2) the SIA coating gradually grew through the heterogeneous conversion of gaseous
365 precursors (e.g., SO₂ and NO_x) in the polluted air. Therefore, aging processes of individual POT
366 particles in wintertime haze well reflect the regional haze evolution in the NCP.

367 **3.5 Changes in light absorption of the POT particles**

368 It is well known that organic aerosols emitted from the coal and biomass burning are the main
369 source of light-absorbing BrC (M. Li et al., 2019; Lin et al., 2016; Sun et al., 2017). Recently, some
370 observation and modeling works show that the BrC in haze layers over the NCP can affect the regional
371 energy budget (Feng et al., 2013; Wang et al., 2018; Xie et al., 2019). However, there is no answer on
372 how the aging process of POT particles influence their optical absorption in the regional haze. Here
373 we further explored variations in the optical absorption of individual POT particles using Mie theory
374 following the haze evolution at the GC rural and BJ urban sites (Fig. 9).

375 At the GC rural site, the average ACS of individual POT-containing particles (ACS_{POT-containing})
376 under the actual scenario in the early, middle, and late stages of heavily polluted period were estimated
377 to be 3.09×10^{-14} , 3.97×10^{-14} , and 4.43×10^{-14} m², respectively (Fig. 9a). If all the POT-containing
378 particles were not coated with SIA in each period (i.e., no particle aging scenario), the corresponding
379 average ACS of individual POT particles (ACS_{POT}) were 3.01×10^{-14} , 3.52×10^{-14} , and 3.18×10^{-14} m²,
380 respectively (Fig. 9a). Based on the ratios of ACS_{POT-containing} to ACS_{POT}, we obtained that the E_{abs}
381 were 1.02, 1.12, and 1.39 in the early, middle, and late stages of heavily polluted period, respectively,
382 at the GC rural site (Fig. 9a). Similarly, at the BJ urban site, the E_{abs} were 1.10 and 1.39 in the
383 moderately and heavily polluted periods, respectively, with the corresponding average ACS_{POT-}
384 _{containing} being 2.06×10^{-14} and 3.00×10^{-14} m² and ACS_{POT} being 1.86×10^{-14} and 2.15×10^{-14} m² (Fig.
385 9b). It should be noted that the light absorption capacity of individual POT particles was a little lower



386 at the BJ urban site than that at the GC rural site (Fig. 9), which was mainly attributed to the smaller
387 sizes of POT particles at the BJ urban site (Fig. 7).

388 To better understand the influence of SIA-coating thickness and POT-core diameter on the light
389 absorption of POT–SIA particles, we modeled the variations in E_{abs} of POT–SIA particles (i.e., ratios
390 of $\text{ACS}_{\text{POT-SIA}}$ to $\text{ACS}_{\text{POT pore}}$) with different D_c as a function of D_p/D_c ratios (Fig. 10). The results
391 show that E_{abs} is sensitive to the changes in both D_c and D_p/D_c ratio. When $D_p/D_c < 1.5$, the E_{abs}
392 increases sharply with the increase of D_p/D_c ratio for different POT core sizes; but when $D_p/D_c > 1.5$,
393 the E_{abs} does not show an increase any more for particles with $D_c > 200$ nm, and the E_{abs} is limited to
394 between 1.5 and 2 for particles with D_c ranging from 200 to 1500 nm (Fig. 10). The diameters of the
395 observed POT cores at GC rural and BJ urban sites in this study were mainly in the range of 200 to
396 800 nm (Fig. 7), thus the E_{abs} of the observed POT–SIA particles in the NCP were mostly below 1.75
397 (Fig. 10). All the above results indicate that the atmospheric aging process could significantly improve
398 the light absorption capacity of POT particles along with the evolution of haze episodes due to the
399 “lensing effect” of SIA coating.

400 **4 Conclusions and implications**

401 This study demonstrates that the primary pollutants especially large amounts of POT particles
402 emitted from the residential coal and biomass burning in rural areas initiated the wintertime regional
403 haze episode in the NCP. The presence of abundant POT particles in the atmosphere could further
404 provide surfaces for the heterogeneous reactions promoting the large production of SIA under
405 stagnant metrological conditions with high RH, which further elevated the pollution level. Compared
406 with the tar balls which have been confirmed as BrC with strong light-absorbing capacities in previous
407 studies (Adachi et al., 2019; C. Li et al., 2019; Zhang et al., 2018), the spherical or irregular POT
408 particles observed in this study can better represent various light-absorbing primary organic particles
409 in the wintertime hazes. Therefore, the ubiquitous brown POT particles in the atmosphere of NCP
410 unquestionably affect the energy balance (Feng et al., 2013). We found that the POT particles



411 remained quite stable during the regional transport from the rural areas to urban Beijing in the NCP
412 and were coated with SIA through the atmospheric aging process in the haze layer, which could
413 significantly enhance the light absorption capacity of POT particles via the “lensing effect” of SIA
414 coating. We estimated that the E_{abs} values were within the upper limit of 1.75 in core-shell Mie
415 simulations considering the typical size distribution (200–800 nm) of POT particles in the NCP.
416 Furthermore, Alexander et al. (2008) found plenty of primary brown organic particles with strong
417 light absorption capacity in East Asian outflow, which indicates that the POT particles could be
418 transported over long distances and still retain their strong light-absorbing properties, and thus can
419 affect the regional and even global radiative forcing. Therefore, we highlight that the “lensing effect”,
420 which has been adequately reported on BC particles but not on the POT particles in previous studies,
421 should be further considered on the POT particles in radiative forcing models.

422 The primary pollutants from the intense coal and biomass burning in rural areas can also pose
423 serious threats to human health. In particular, large amounts of toxic primary particles can be released
424 from coal and biomass burning, such as the polycyclic aromatic hydrocarbons (PAHs) in POA and
425 the toxic heavy metals (Cheng et al., 2019; C. Li et al., 2019; X. Wang et al., 2017), which could lead
426 to high concentrations of toxic substances in the rural atmosphere and further be transported in large
427 scale. Recently, Zhao et al. (2018) reported that approximately 80% of premature deaths occurred in
428 the rural areas of China in 2015 was attributed to the $\text{PM}_{2.5}$ released from household fuels.

429 Considering the adverse effects of residential coal and biomass burning on the haze formation,
430 human health, and climate change, we suggest that the governments should continue to implement
431 the “Clean Air Actions” (Zhang and Geng, 2019), especially encourage the use of clean energy such
432 as electricity and natural gas for heating and cooking in rural areas of North China in winter.

433 **Data availability**

434 All data presented in this paper are available upon request. Please contact the corresponding
435 author (liweijun@zju.edu.cn).



436 **Author Contributions**

437 WL and LL designed the research. LL performed the data analysis and wrote the manuscript and
438 WL revised it. JZ and YZ assisted with the sample collection. YS provided the AMS data at the
439 Beijing site. LL, JZ, YZ, LX, QY, and YW carried out the chemical analysis of PM_{2.5} and TEM
440 analysis of individual particles. ZS, YS, DL, and PF contributed to the improvement of this
441 manuscript. All the authors approved the final version of this paper.

442 **Competing interests**

443 The authors declare that they have no conflict of interest.

444 **Acknowledgements**

445 This work was funded by the National Key R&D Program of China (2017YFC0212700),
446 National Natural Science Foundation of China (42075096, 91844301), and Zhejiang Provincial
447 Natural Science Foundation of China (LZ19D050001). Z. Shi acknowledges the UK Natural
448 Environment Research Council (NE/S00579X/1 and NE/N007190/1). We acknowledge the NOAA
449 Air Resources Laboratory for the provision of the HYSPLIT transport and dispersion model and
450 READY website (<http://www.ready.noaa.gov>) used in this paper.

451 **References**

- 452 Adachi, K., Sedlacek, A. J., Kleinman, L., Chand, D., Hubbe, J. M., and Buseck, P. R.: Volume
453 changes upon heating of aerosol particles from biomass burning using transmission electron
454 microscopy, *Aerosol Sci. Tech.*, 52, 46-56, 10.1080/02786826.2017.1373181, 2018.
- 455 Adachi, K., Sedlacek, A. J., Kleinman, L., Springston, S. R., Wang, J., Chand, D., Hubbe, J. M.,
456 Shilling, J. E., Onasch, T. B., Kinase, T., Sakata, K., Takahashi, Y., and Buseck, P. R.: Spherical
457 tarball particles form through rapid chemical and physical changes of organic matter in biomass-
458 burning smoke, *Proc. Natl. Acad. Sci. U.S.A.*, 116, 19336-19341, 10.1073/pnas.1900129116,
459 2019.
- 460 Alexander, D. T. L., Crozier, P. A., and Anderson, J. R.: Brown carbon spheres in East Asian outflow
461 and their optical properties, *Science*, 321, 833-836, 2008.
- 462 Bohren, C. F., and Huffman, D. R.: Absorption and scattering of light by small particles, John Wiley



- 463 & Sons, New York, 1983.
- 464 Bond, T. C., Doherty, S. J., Fahey, D., Forster, P., Berntsen, T., DeAngelo, B., Flanner, M., Ghan, S.,
465 Kärcher, B., and Koch, D.: Bounding the role of black carbon in the climate system: A scientific
466 assessment, *J. Geophys. Res.-Atmos.*, 118, 5380-5552, 2013.
- 467 Chakrabarty, R. K., and Heinson, W. R.: Scaling Laws for Light Absorption Enhancement Due to
468 Nonrefractory Coating of Atmospheric Black Carbon Aerosol, *Phys. Rev. Lett.*, 121, 218701,
469 10.1103/PhysRevLett.121.218701, 2018.
- 470 Chang, X., Wang, S., Zhao, B., Cai, S., and Hao, J.: Assessment of inter-city transport of particulate
471 matter in the Beijing–Tianjin–Hebei region, *Atmos. Chem. Phys.*, 18, 4843-4858, 10.5194/acp-
472 18-4843-2018, 2018.
- 473 Chen, S., Xu, L., Zhang, Y., Chen, B., Wang, X., Zhang, X., Zheng, M., Chen, J., Wang, W., Sun, Y.,
474 Fu, P., Wang, Z., and Li, W.: Direct observations of organic aerosols in common wintertime hazes
475 in North China: insights into direct emissions from Chinese residential stoves, *Atmos. Chem.*
476 *Phys.*, 17, 1259-1270, 10.5194/acp-17-1259-2017, 2017.
- 477 Chen, X., Wang, H., Lu, K., Li, C., Zhai, T., Tan, Z., Ma, X., Yang, X., Liu, Y., Chen, S., Dong, H.,
478 Li, X., Wu, Z., Hu, M., Zeng, L., and Zhang, Y.: Field Determination of Nitrate Formation
479 Pathway in Winter Beijing, *Environ. Sci. Technol.*, 54, 9243-9253, 10.1021/acs.est.0c00972, 2020.
- 480 Cheng, Y., Zheng, G., Wei, C., Mu, Q., Zheng, B., Wang, Z., Gao, M., Zhang, Q., He, K., Carmichael,
481 G., Pöschl, U., and Su, H.: Reactive nitrogen chemistry in aerosol water as a source of sulfate
482 during haze events in China, *Sci. Adv.*, 2, e1601530, 10.1126/sciadv.1601530, 2016.
- 483 Cheng, Y., Kong, S., Yan, Q., Liu, H., Wang, W., Chen, K., Yin, Y., Zheng, H., Wu, J., Yao, L., Zeng,
484 X., Zheng, S., Wu, F., Niu, Z., Zhang, Y., Yan, Y., Zheng, M., and Qi, S.: Size-segregated emission
485 factors and health risks of PAHs from residential coal flaming/smoldering combustion, *Environ.*
486 *Sci. Pollut. Res.*, 26, 31793-31803, 10.1007/s11356-019-06340-2, 2019.
- 487 Chylek, P., Lee, J. E., Romonosky, D. E., Gallo, F., Lou, S., Shrivastava, M., Carrico, C. M., Aiken,
488 A. C., and Dubey, M. K.: Mie Scattering Captures Observed Optical Properties of Ambient
489 Biomass Burning Plumes Assuming Uniform Black, Brown, and Organic Carbon Mixtures, *J.*
490 *Geophys. Res.-Atmos.*, 124, 11406-11427, 10.1029/2019jd031224, 2019.
- 491 Denjean, C., Formenti, P., Picquet-Varrault, B., Katrib, Y., Pangui, E., Zapf, P., and Doussin, J. F.: A
492 new experimental approach to study the hygroscopic and optical properties of aerosols:
493 application to ammonium sulfate particles, *Atmos. Meas. Tech.*, 7, 183-197, 10.5194/amt-7-183-
494 2014, 2014.
- 495 Du, H., Li, J., Chen, X., Wang, Z., Sun, Y., Fu, P., Li, J., Gao, J., and Wei, Y.: Modeling of aerosol
496 property evolution during winter haze episodes over a megacity cluster in northern China: roles



- 497 of regional transport and heterogeneous reactions of SO₂, *Atmos. Chem. Phys.*, 19, 9351-9370,
498 10.5194/acp-19-9351-2019, 2019.
- 499 Ebert, M., Weigel, R., Kandler, K., Günther, G., Molleker, S., Groß, J. U., Vogel, B., Weinbruch, S.,
500 and Borrmann, S.: Chemical analysis of refractory stratospheric aerosol particles collected within
501 the arctic vortex and inside polar stratospheric clouds, *Atmos. Chem. Phys.*, 16, 8405-8421,
502 10.5194/acp-16-8405-2016, 2016.
- 503 Fan, X., Liu, J., Zhang, F., Chen, L., Collins, D., Xu, W., Jin, X., Ren, J., Wang, Y., Wu, H., Li, S.,
504 Sun, Y., and Li, Z.: Contrasting size-resolved hygroscopicity of fine particles derived by HTDMA
505 and HR-ToF-AMS measurements between summer and winter in Beijing: the impacts of aerosol
506 aging and local emissions, *Atmos. Chem. Phys.*, 20, 915-929, 10.5194/acp-20-915-2020, 2020.
- 507 Feng, Y., Ramanathan, V., and Kotamarthi, V. R.: Brown carbon: a significant atmospheric absorber
508 of solar radiation?, *Atmos. Chem. Phys.*, 13, 8607-8621, 10.5194/acp-13-8607-2013, 2013.
- 509 IPCC: Climate change 2013: The Physical Science Basis. Contribution of Working Group I to the
510 Fifth Assessment Report of the Intergovernmental Panel on Climate Change, Cambridge
511 University Press, Cambridge/New York, 2013.
- 512 Li, C., He, Q., Schade, J., Passig, J., Zimmermann, R., Meidan, D., Laskin, A., and Rudich, Y.:
513 Dynamic changes in optical and chemical properties of tar ball aerosols by atmospheric
514 photochemical aging, *Atmos. Chem. Phys.*, 19, 139-163, 10.5194/acp-19-139-2019, 2019.
- 515 Li, H., Zhang, Q., Zhang, Q., Chen, C., Wang, L., Wei, Z., Zhou, S., Parworth, C., Zheng, B.,
516 Canonaco, F., Prevot, A. S. H., Chen, P., Zhang, H., Wallington, T. J., and He, K.: Wintertime
517 aerosol chemistry and haze evolution in an extremely polluted city of the North China Plain:
518 significant contribution from coal and biomass combustion, *Atmos. Chem. Phys.*, 17, 4751-4768,
519 10.5194/acp-17-4751-2017, 2017.
- 520 Li, J., Han, Z., Li, J., Liu, R., Wu, Y., Liang, L., and Zhang, R.: The formation and evolution of
521 secondary organic aerosol during haze events in Beijing in wintertime, *Sci. Total Environ.*, 703,
522 134937, 10.1016/j.scitotenv.2019.134937, 2020.
- 523 Li, M., Fan, X., Zhu, M., Zou, C., Song, J., Wei, S., Jia, W., and Peng, P. a.: Abundance and Light
524 Absorption Properties of Brown Carbon Emitted from Residential Coal Combustion in China,
525 *Environ. Sci. Technol.*, 53, 595-603, 10.1021/acs.est.8b05630, 2019.
- 526 Li, W., Zhou, S., Wang, X., Xu, Z., Yuan, C., Yu, Y., Zhang, Q., and Wang, W.: Integrated evaluation
527 of aerosols from regional brown hazes over northern China in winter: Concentrations, sources,
528 transformation, and mixing states, *J. Geophys. Res.-Atmos.*, 116, D09301,
529 10.1029/2010JD015099, 2011.
- 530 Li, W., Shao, L., Zhang, D., Ro, C.-U., Hu, M., Bi, X., Geng, H., Matsuki, A., Niu, H., and Chen, J.:



- 531 A review of single aerosol particle studies in the atmosphere of East Asia: morphology, mixing
532 state, source, and heterogeneous reactions, *J. Clean Prod.*, 112, 1330-1349,
533 10.1016/j.jclepro.2015.04.050, 2016a.
- 534 Li, W., Sun, J., Xu, L., Shi, Z., Riemer, N., Sun, Y., Fu, P., Zhang, J., Lin, Y., and Wang, X.: A
535 conceptual framework for mixing structures in individual aerosol particles, *J. Geophys. Res.-*
536 *Atmos.*, 121, 13784-13798, 10.1002/2016JD025252, 2016b.
- 537 Li, X., Yang, Y., Liu, S., Zhao, Q., Wang, G., and Wang, Y.: Light absorption properties of brown
538 carbon (BrC) in autumn and winter in Beijing: Composition, formation and contribution of
539 nitrated aromatic compounds, *Atmos. Environ.*, 223, 117289, 10.1016/j.atmosenv.2020.117289,
540 2020.
- 541 Lin, P., Aiona, P. K., Li, Y., Shiraiwa, M., Laskin, J., Nizkorodov, S. A., and Laskin, A.: Molecular
542 Characterization of Brown Carbon in Biomass Burning Aerosol Particles, *Environ. Sci. Technol.*,
543 50, 11815-11824, 10.1021/acs.est.6b03024, 2016.
- 544 Liu, D., Whitehead, J., Alfarra, M. R., Reyes-Villegas, E., Spracklen, D. V., Reddington, C. L., Kong,
545 S., Williams, P. I., Ting, Y.-C., Haslett, S., Taylor, J. W., Flynn, M. J., Morgan, W. T., McFiggans,
546 G., Coe, H., and Allan, J. D.: Black-carbon absorption enhancement in the atmosphere determined
547 by particle mixing state, *Nat. Geosci.*, 10, 184-188, 10.1038/ngeo2901, 2017.
- 548 Liu, J., Mauzerall, D. L., Chen, Q., Zhang, Q., Song, Y., Peng, W., Klimont, Z., Qiu, X., Zhang, S.,
549 Hu, M., Lin, W., Smith, K. R., and Zhu, T.: Air pollutant emissions from Chinese households: A
550 major and underappreciated ambient pollution source, *Proc. Natl. Acad. Sci. U.S.A.*, 113, 7756-
551 7761, 10.1073/pnas.1604537113, 2016.
- 552 Liu, L., Kong, S., Zhang, Y., Wang, Y., Xu, L., Yan, Q., Lingaswamy, A. P., Shi, Z., Lv, S., Niu, H.,
553 Shao, L., Hu, M., Zhang, D., Chen, J., Zhang, X., and Li, W.: Morphology, composition, and
554 mixing state of primary particles from combustion sources — crop residue, wood, and solid waste,
555 *Sci. Rep.*, 7, 5047, 10.1038/s41598-017-05357-2, 2017.
- 556 Liu, L., Zhang, J., Xu, L., Yuan, Q., Huang, D., Chen, J., Shi, Z., Sun, Y., Fu, P., Wang, Z. F., Zhang,
557 D., and Li, W.: Cloud scavenging of anthropogenic refractory particles at a mountain site in North
558 China, *Atmos. Chem. Phys.*, 18, 14681-14693, 10.5194/acp-18-14681-2018, 2018.
- 559 Liu, P., Zhang, C., Xue, C., Mu, Y., Liu, J., Zhang, Y., Tian, D., Ye, C., Zhang, H., and Guan, J.: The
560 contribution of residential coal combustion to atmospheric PM_{2.5} in northern China during winter,
561 *Atmos. Chem. Phys.*, 17, 11503-11520, 10.5194/acp-17-11503-2017, 2017.
- 562 Liu, P., Ye, C., Xue, C., Zhang, C., Mu, Y., and Sun, X.: Formation mechanisms of atmospheric nitrate
563 and sulfate during the winter haze pollution periods in Beijing: gas-phase, heterogeneous and
564 aqueous-phase chemistry, *Atmos. Chem. Phys.*, 20, 4153-4165, 10.5194/acp-20-4153-2020, 2020.



- 565 Ma, Q., Wu, Y., Zhang, D., Wang, X., Xia, Y., Liu, X., Tian, P., Han, Z., Xia, X., Wang, Y., and Zhang,
566 R.: Roles of regional transport and heterogeneous reactions in the PM_{2.5} increase during winter
567 haze episodes in Beijing, *Sci. Total Environ.*, 599–600, 246–253, 10.1016/j.scitotenv.2017.04.193,
568 2017.
- 569 Pósfai, M., Simonics, R., Li, J., Hobbs, P. V., and Buseck, P. R.: Individual aerosol particles from
570 biomass burning in southern Africa: 1. Compositions and size distributions of carbonaceous
571 particles, *J. Geophys. Res.-Atmos.*, 108, 8483, 10.1029/2002JD002291, 2003.
- 572 Reid, J. P., Bertram, A. K., Topping, D. O., Laskin, A., Martin, S. T., Petters, M. D., Pope, F. D., and
573 Rovelli, G.: The viscosity of atmospherically relevant organic particles, *Nat. Commun.*, 9, 956,
574 10.1038/s41467-018-03027-z, 2018.
- 575 Riemer, N., Ault, A. P., West, M., Craig, R. L., and Curtis, J. H.: Aerosol Mixing State: Measurements,
576 Modeling, and Impacts, *Rev. Geophys.*, 57, 187–249, 10.1029/2018rg000615, 2019.
- 577 Seinfeld, J. H., and Pandis, S. N.: *Atmospheric chemistry and physics: from air pollution to climate
578 change*, John Wiley & Sons, 2006.
- 579 Shi, Z., Vu, T., Kotthaus, S., Harrison, R. M., Grimmond, S., Yue, S., Zhu, T., Lee, J., Han, Y.,
580 Demuzere, M., Dunmore, R. E., Ren, L., Liu, D., Wang, Y., Wild, O., Allan, J., Acton, W. J.,
581 Barlow, J., Barratt, B., Beddows, D., Bloss, W. J., Calzolari, G., Carruthers, D., Carslaw, D. C.,
582 Chan, Q., Chatzidiakou, L., Chen, Y., Crilley, L., Coe, H., Dai, T., Doherty, R., Duan, F., Fu, P.,
583 Ge, B., Ge, M., Guan, D., Hamilton, J. F., He, K., Heal, M., Heard, D., Hewitt, C. N., Holloway,
584 M., Hu, M., Ji, D., Jiang, X., Jones, R., Kalberer, M., Kelly, F. J., Kramer, L., Langford, B., Lin,
585 C., Lewis, A. C., Li, J., Li, W., Liu, H., Liu, J., Loh, M., Lu, K., Lucarelli, F., Mann, G., McFiggans,
586 G., Miller, M. R., Mills, G., Monk, P., Nemitz, E., O'Connor, F., Ouyang, B., Palmer, P. I., Percival,
587 C., Popoola, O., Reeves, C., Rickard, A. R., Shao, L., Shi, G., Spracklen, D., Stevenson, D., Sun,
588 Y., Sun, Z., Tao, S., Tong, S., Wang, Q., Wang, W., Wang, X., Wang, X., Wang, Z., Wei, L.,
589 Whalley, L., Wu, X., Wu, Z., Xie, P., Yang, F., Zhang, Q., Zhang, Y., Zhang, Y., and Zheng, M.:
590 Introduction to the special issue “In-depth study of air pollution sources and processes within
591 Beijing and its surrounding region (APHH-Beijing)”, *Atmos. Chem. Phys.*, 19, 7519–7546,
592 10.5194/acp-19-7519-2019, 2019.
- 593 Song, J., Li, M., Jiang, B., Wei, S., Fan, X., and Peng, P. a.: Molecular Characterization of Water-
594 Soluble Humic like Substances in Smoke Particles Emitted from Combustion of Biomass
595 Materials and Coal Using Ultrahigh-Resolution Electrospray Ionization Fourier Transform Ion
596 Cyclotron Resonance Mass Spectrometry, *Environ. Sci. Technol.*, 52, 2575–2585,
597 10.1021/acs.est.7b06126, 2018.
- 598 Stein, A. F., Draxler, R. R., Rolph, G. D., Stunder, B. J. B., Cohen, M. D., and Ngan, F.: NOAA's



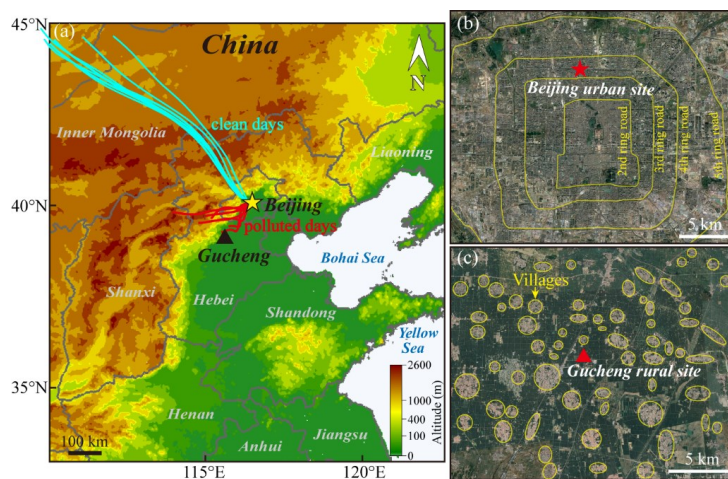
- 599 HYSPLIT Atmospheric Transport and Dispersion Modeling System, *Bull. Amer. Meteorol. Soc.*,
600 96, 2059-2077, 10.1175/bams-d-14-00110.1, 2016.
- 601 Sun, J., Zhi, G., Hitzenberger, R., Chen, Y., Tian, C., Zhang, Y., Feng, Y., Cheng, M., Zhang, Y., Cai,
602 J., Chen, F., Qiu, Y., Jiang, Z., Li, J., Zhang, G., and Mo, Y.: Emission factors and light absorption
603 properties of brown carbon from household coal combustion in China, *Atmos. Chem. Phys.*, 17,
604 4769-4780, 10.5194/acp-17-4769-2017, 2017.
- 605 Sun, Y., Jiang, Q., Wang, Z., Fu, P., Li, J., Yang, T., and Yin, Y.: Investigation of the sources and
606 evolution processes of severe haze pollution in Beijing in January 2013, *J. Geophys. Res.-Atmos.*,
607 119, 4380-4398, 10.1002/2014jd021641, 2014.
- 608 Sun, Y., Chen, C., Zhang, Y., Xu, W., Zhou, L., Cheng, X., Zheng, H., Ji, D., Li, J., Tang, X., Fu, P.,
609 and Wang, Z.: Rapid formation and evolution of an extreme haze episode in Northern China
610 during winter 2015, *Sci. Rep.*, 6, 27151, 10.1038/srep27151, 2016.
- 611 Wang, B., Harder, T. H., Kelly, S. T., Piens, D. S., China, S., Kovarik, L., Keiluweit, M., Arey, B. W.,
612 Gilles, M. K., and Laskin, A.: Airborne soil organic particles generated by precipitation, *Nat.*
613 *Geosci.*, 9, 433-437, 10.1038/NGEO2705, 2016.
- 614 Wang, J., Nie, W., Cheng, Y., Shen, Y., Chi, X., Wang, J., Huang, X., Xie, Y., Sun, P., Xu, Z., Qi, X.,
615 Su, H., and Ding, A.: Light absorption of brown carbon in eastern China based on 3-year multi-
616 wavelength aerosol optical property observations and an improved absorption Ångström exponent
617 segregation method, *Atmos. Chem. Phys.*, 18, 9061-9074, 10.5194/acp-18-9061-2018, 2018.
- 618 Wang, J., Li, J., Ye, J., Zhao, J., Wu, Y., Hu, J., Liu, D., Nie, D., Shen, F., Huang, X., Huang, D. D.,
619 Ji, D., Sun, X., Xu, W., Guo, J., Song, S., Qin, Y., Liu, P., Turner, J. R., Lee, H. C., Hwang, S.,
620 Liao, H., Martin, S. T., Zhang, Q., Chen, M., Sun, Y., Ge, X., and Jacob, D. J.: Fast sulfate
621 formation from oxidation of SO₂ by NO₂ and HONO observed in Beijing haze, *Nat. Commun.*,
622 11, 2844, 10.1038/s41467-020-16683-x, 2020.
- 623 Wang, X., Heald, C. L., Ridley, D. A., Schwarz, J. P., Spackman, J. R., Perring, A. E., Coe, H., Liu,
624 D., and Clarke, A. D.: Exploiting simultaneous observational constraints on mass and absorption
625 to estimate the global direct radiative forcing of black carbon and brown carbon, *Atmos. Chem.*
626 *Phys.*, 14, 10989-11010, 10.5194/acp-14-10989-2014, 2014.
- 627 Wang, X., Gu, R., Wang, L., Xu, W., Zhang, Y., Chen, B., Li, W., Xue, L., Chen, J., and Wang, W.:
628 Emissions of fine particulate nitrated phenols from the burning of five common types of biomass,
629 *Environ. Pollut.*, 230, 405-412, 10.1016/j.envpol.2017.06.072, 2017.
- 630 Wang, Y., Liu, F., He, C., Bi, L., Cheng, T., Wang, Z., Zhang, H., Zhang, X., Shi, Z., and Li, W.:
631 Fractal Dimensions and Mixing Structures of Soot Particles during Atmospheric Processing,
632 *Environ. Sci. Technol. Lett.*, 4, 487-493, 10.1021/acs.estlett.7b00418, 2017.



- 633 West, J. J., Cohen, A., Dentener, F., Brunekreef, B., Zhu, T., Armstrong, B., Bell, M. L., Brauer, M.,
634 Carmichael, G., and Costa, D. L.: What We Breathe Impacts Our Health: Improving
635 Understanding of the Link between Air Pollution and Health, *Environ. Sci. Technol.*, 50, 4895-
636 4904, 10.1021/acs.est.5b03827, 2016.
- 637 Wu, C., Wu, D., and Yu, J. Z.: Quantifying black carbon light absorption enhancement with a novel
638 statistical approach, *Atmos. Chem. Phys.*, 18, 289-309, 10.5194/acp-18-289-2018, 2018.
- 639 Xie, C., Xu, W., Wang, J., Wang, Q., Liu, D., Tang, G., Chen, P., Du, W., Zhao, J., Zhang, Y., Zhou,
640 W., Han, T., Bian, Q., Li, J., Fu, P., Wang, Z., Ge, X., Allan, J., Coe, H., and Sun, Y.: Vertical
641 characterization of aerosol optical properties and brown carbon in winter in urban Beijing, China,
642 *Atmos. Chem. Phys.*, 19, 165-179, 10.5194/acp-19-165-2019, 2019.
- 643 Xing, L., Fu, T. M., Cao, J. J., Lee, S. C., Wang, G. H., Ho, K. F., Cheng, M. C., You, C. F., and Wang,
644 T. J.: Seasonal and spatial variability of the OM/OC mass ratios and high regional correlation
645 between oxalic acid and zinc in Chinese urban organic aerosols, *Atmos. Chem. Phys.*, 13, 4307-
646 4318, 10.5194/acp-13-4307-2013, 2013.
- 647 Xu, J., Srivastava, D., Wu, X., Hou, S., Vu, T. V., Liu, D., Sun, Y., Vlachou, A., Moschos, V., Salazar,
648 G., Szidat, S., Prevot, A., Fu, P., Harrison, R. M., and Shi, Z.: An evaluation of source
649 apportionment of fine OC and PM_{2.5} by multiple methods: APHH-Beijing campaigns as a case
650 study, *Faraday Discussions*, 10.1039/D0FD00095G, 2020.
- 651 Xu, W., Sun, Y., Wang, Q., Zhao, J., Wang, J., Ge, X., Xie, C., Zhou, W., Du, W., Li, J., Fu, P., Wang,
652 Z., Worsnop, D. R., and Coe, H.: Changes in Aerosol Chemistry From 2014 to 2016 in Winter in
653 Beijing: Insights From High-Resolution Aerosol Mass Spectrometry, *J. Geophys. Res.-Atmos.*,
654 124, 1132-1147, 10.1029/2018jd029245, 2019.
- 655 Yan, C., Zheng, M., Bosch, C., Andersson, A., Desyaterik, Y., Sullivan, A. P., Collett, J. L., Zhao, B.,
656 Wang, S., He, K., and Gustafsson, Ö.: Important fossil source contribution to brown carbon in
657 Beijing during winter, *Sci. Rep.*, 7, 43182, 10.1038/srep43182, 2017.
- 658 Yu, H., Li, W., Zhang, Y., Tunved, P., Dall'Osto, M., Shen, X., Sun, J., Zhang, X., Zhang, J., and Shi,
659 Z.: Organic coating on sulfate and soot particles during late summer in the Svalbard Archipelago,
660 *Atmos. Chem. Phys.*, 19, 10433-10446, 10.5194/acp-19-10433-2019, 2019.
- 661 Zhang, J., Liu, L., Wang, Y., Ren, Y., Wang, X., Shi, Z., Zhang, D., Che, H., Zhao, H., Liu, Y., Niu,
662 H., Chen, J., Zhang, X., Lingaswamy, A. P., Wang, Z., and Li, W.: Chemical composition, source,
663 and process of urban aerosols during winter haze formation in Northeast China, *Environ. Pollut.*,
664 231, 357-366, 10.1016/j.envpol.2017.07.102, 2017.
- 665 Zhang, J., Liu, L., Xu, L., Lin, Q., Zhao, H., Wang, Z., Guo, S., Hu, M., Liu, D., Shi, Z., Huang, D.,
666 and Li, W.: Exploring wintertime regional haze in northeast China: role of coal and biomass

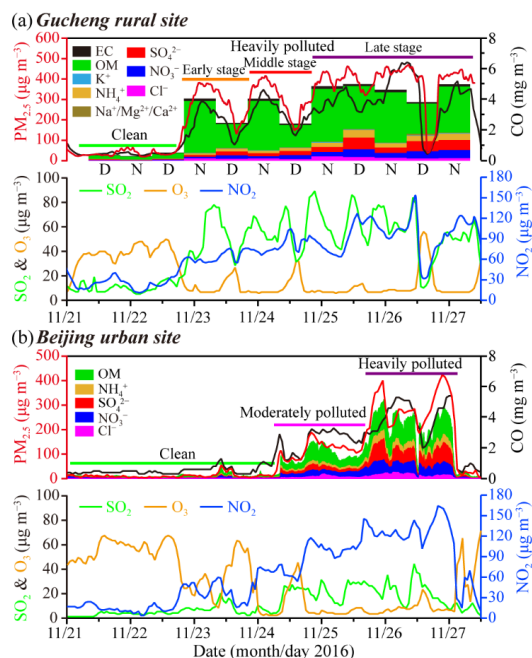


- 667 burning, *Atmos. Chem. Phys.*, 20, 5355-5372, 10.5194/acp-20-5355-2020, 2020.
- 668 Zhang, Q., and Geng, G.: Impact of clean air action on PM_{2.5} pollution in China, *Sci. China-Earth*
669 *Sci.*, 62, 1845, 10.1007/s11430-019-9531-4, 2019.
- 670 Zhang, Y., Yuan, Q., Huang, D., Kong, S., Zhang, J., Wang, X., Lu, C., Shi, Z., Zhang, X., Sun, Y.,
671 Wang, Z., Shao, L., Zhu, J., and Li, W.: Direct observations of fine primary particles from
672 residential coal burning: insights into their morphology, composition, and hygroscopicity, *J.*
673 *Geophys. Res.-Atmos.*, 123, 12964-12979, 10.1029/2018JD028988, 2018.
- 674 Zhao, B., Zheng, H., Wang, S., Smith, K. R., Lu, X., Aunan, K., Gu, Y., Wang, Y., Ding, D., Xing, J.,
675 Fu, X., Yang, X., Liou, K.-N., and Hao, J.: Change in household fuels dominates the decrease in
676 PM_{2.5} exposure and premature mortality in China in 2005-2015, *Proc. Natl. Acad. Sci. U.S.A.*,
677 115, 12401-12406, 10.1073/pnas.1812955115, 2018.
- 678 Zheng, G. J., Duan, F. K., Su, H., Ma, Y. L., Cheng, Y., Zheng, B., Zhang, Q., Huang, T., Kimoto, T.,
679 Chang, D., Pöschl, U., Cheng, Y. F., and He, K. B.: Exploring the severe winter haze in Beijing:
680 the impact of synoptic weather, regional transport and heterogeneous reactions, *Atmos. Chem.*
681 *Phys.*, 15, 2969-2983, 10.5194/acp-15-2969-2015, 2015.
- 682 Zhong, J., Zhang, X., Wang, Y., Wang, J., Shen, X., Zhang, H., Wang, T., Xie, Z., Liu, C., Zhang, H.,
683 Zhao, T., Sun, J., Fan, S., Gao, Z., Li, Y., and Wang, L.: The two-way feedback mechanism
684 between unfavorable meteorological conditions and cumulative aerosol pollution in various haze
685 regions of China, *Atmos. Chem. Phys.*, 19, 3287-3306, 10.5194/acp-19-3287-2019, 2019.
- 686



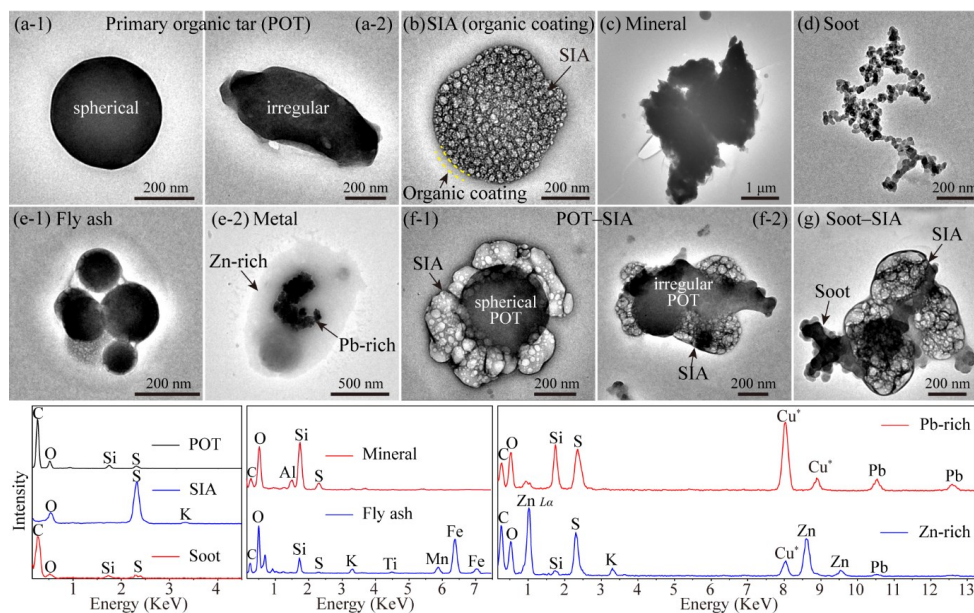
687

688 Figure 1. Locations of Beijing and Gucheng in the North China Plain (a) and the expanded view of surrounding
689 topographies around the Beijing urban site (b) and Gucheng rural site (c). The 24-h backward trajectories of air
690 masses ending at the height of 100 m (a.g.l) over the Beijing urban site in clean and polluted days during 20–27
691 November, 2020 are also shown in (a). (Map copyright ©2020 Google Maps)



692

693 Figure 2. Time series of $PM_{2.5}$, aerosol chemical species, and gaseous pollutants (i.e., CO, SO_2 , O_3 , and NO_2) at the
694 (a) Gucheng rural site and (b) Beijing urban site. Chemical species at the rural site were obtained by offline analysis
695 of daytime (D) and nighttime (N) $PM_{2.5}$ filter samples. Chemical species at the urban site were obtained by online
696 analysis of NR- PM_{10} using a high-resolution aerosol mass spectrometer (HR-AMS). The different periods of the
697 haze episode at rural and urban sites are marked in this figure.



698

699

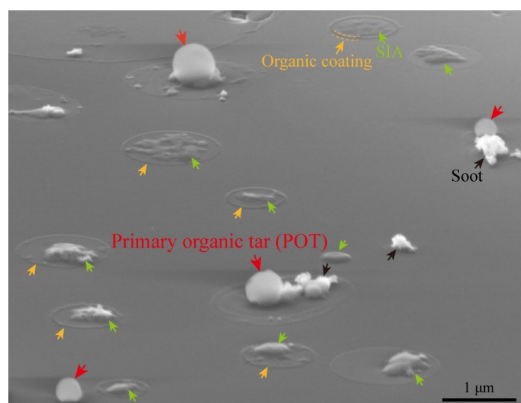
700

701

702

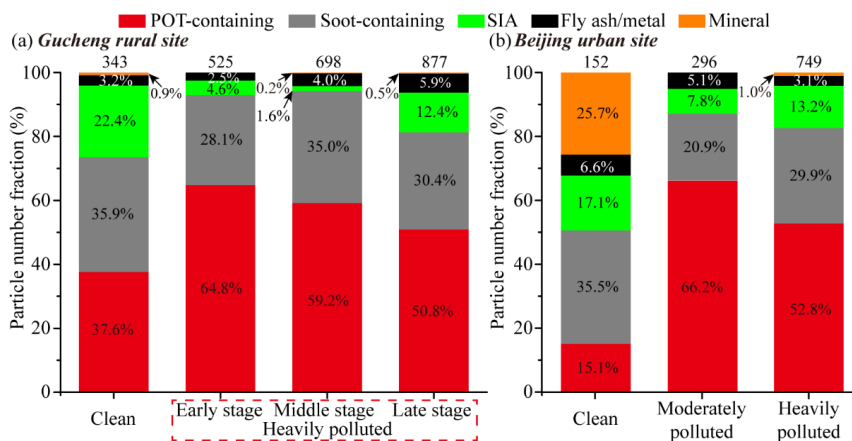
703

Figure 3. Typical transmission electron microscopy (TEM) images and energy-dispersive X-ray spectrometry (EDS) spectra showing the morphology, composition, and mixing structures of different individual particle types. (a) primary organic tar (POT) particles with (a-1) spherical and (a-2) irregular shapes; (b) secondary inorganic aerosol (SIA) particle with secondary organic coating; (c) mineral; (d) soot; (e-1) fly ash and (e-2) metal; (f) internally mixed POT particle with SIA coating (POT-SIA); (g) internally mixed soot particle with SIA coating (soot-SIA).



704

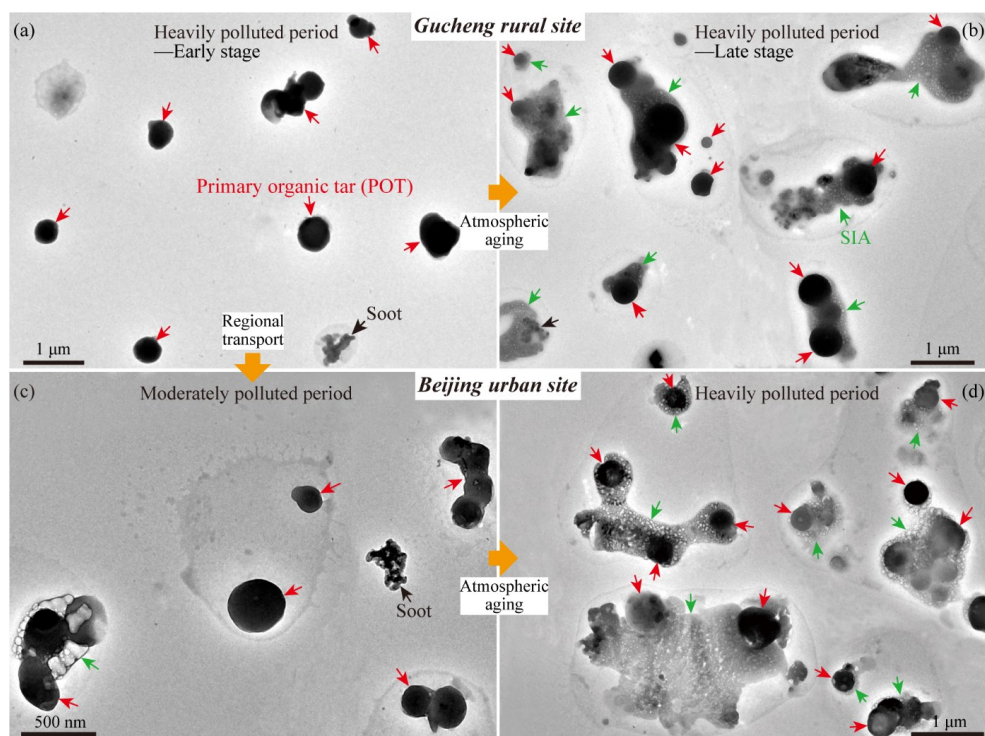
705 Figure 4. Scanning electron microscopy (SEM) image acquired in the secondary electron (SE2) mode at a 75° tilt
706 angle showing the surface morphology of individual particles in the vertical dimension. The red, black, green, and
707 orange arrows indicate the primary organic tar (POT) particle, soot particle, secondary inorganic aerosol (SIA)
708 particle, and secondary organic coating, respectively.



709

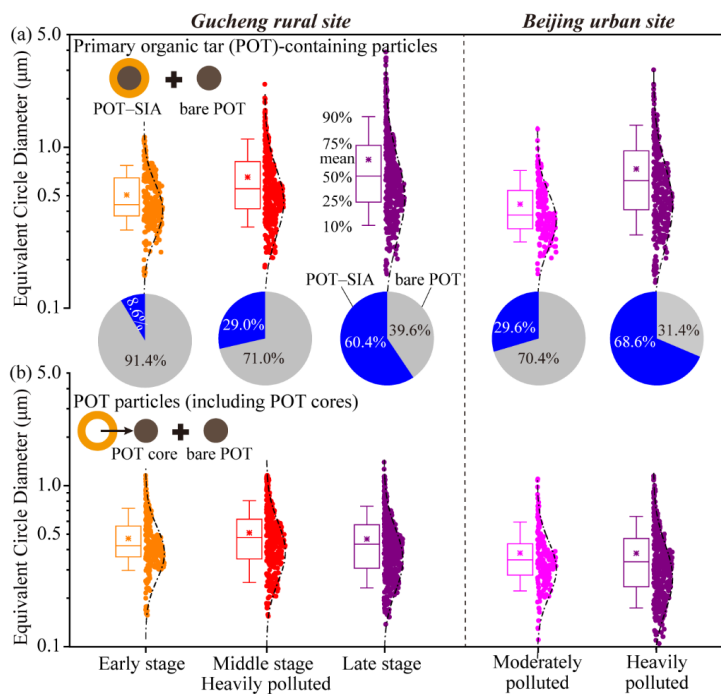
710 Figure 5. Relative abundance of different particle types in different periods at the (a) Gucheng rural site and (b)

711 Beijing urban site. The numbers of analyzed particles in different periods are shown on the top of each column.



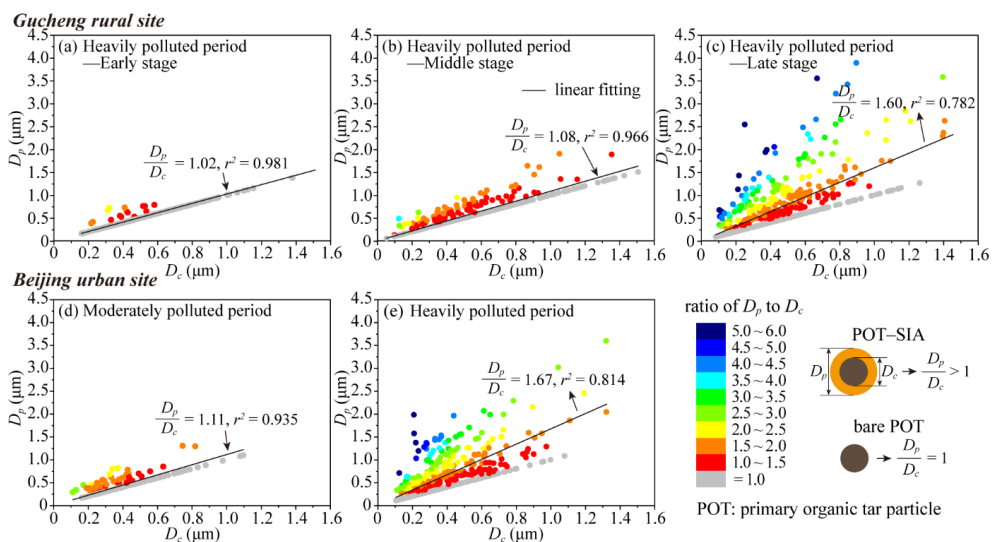
712

713 Figure 6. TEM images showing individual particles collected in the (a) early stage and (b) late stage of heavily
714 polluted period at the Gucheng rural site and in the (c) moderately polluted and (d) heavily polluted periods at the
715 Beijing urban site. The red, green, and black arrows indicate the primary organic tar (POT) particle, secondary
716 inorganic aerosol (SIA) particle, and soot particle, respectively.



717

718 Figure 7. Box plots of equivalent circle diameters (ECD) of (a) primary organic tar (POT)-containing particles (i.e.,
 719 coated POT with secondary inorganic aerosol shell (named as POT-SIA) and bare POT) and (b) POT particles
 720 (including POT cores and bare POT) in different polluted periods at the Gucheng rural site and Beijing urban site.
 721 The solid circles (right of the box) represent the ECD of individual particles with lognormal distributions. The pie
 722 charts present the variation in relative number fractions between POT-SIA and bare POT in different polluted
 723 periods.

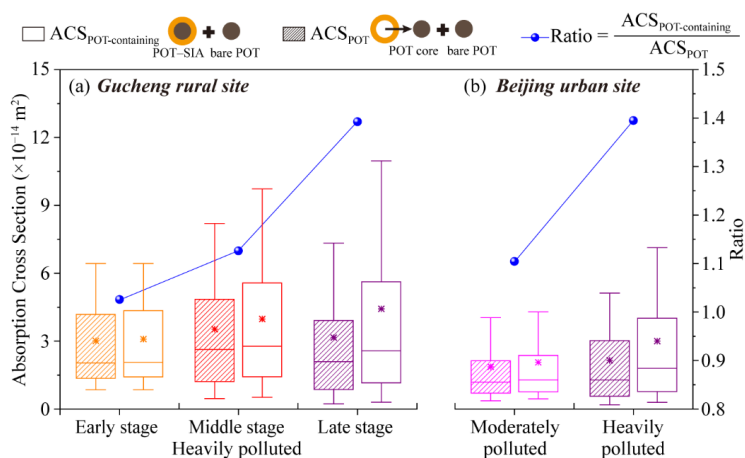


724

725 Figure 8. Relationship between the diameter of POT-containing particle (D_p) and its POT core (D_c) in the (a) early

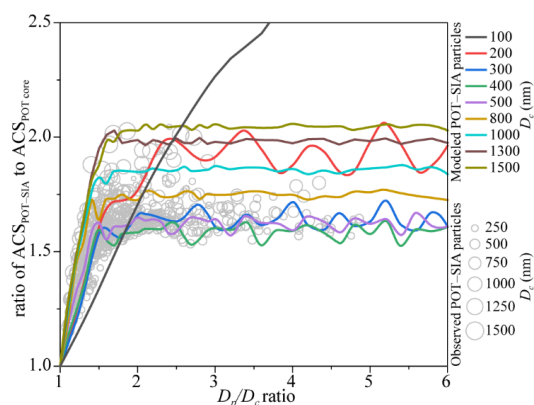
726 stage, (b) middle stage, and (c) late stage of heavily polluted period at the Gucheng rural site and in the (d)

727 moderately polluted and (e) heavily polluted periods at the Beijing urban site.



728

729 Figure 9. Box plots of absorption cross sections (ACS) of individual POT-containing
 730 particles (i.e., $ACS_{POT-containing}$ under the actual scenario) and POT particles (including POT cores, i.e., ACS_{POT}
 731 under the no particle aging scenario), and the variation in the ratios of $ACS_{POT-containing}$ to ACS_{POT} in different polluted periods at the (a) Gucheng rural site
 732 and (b) Beijing urban site. The box represents the 25th (lower line), 50th (middle line), and 75th (top line) percentiles;
 733 the asterisk in the box represents the mean value; the end lines of the vertical bars represent the 10th (below the
 734 box) and 90th (above the box) percentiles.



735

736 Figure 10. Mie-simulated light absorption enhancements (E_{abs}) of modeled POT-SIA particles (i.e., ratio of ACS_{POT-SIA}
737 SIA to ACS_{POT-core}) with different POT core diameters (D_c) as a function of particle-to-core ratio (D_p/D_c ratio) at the
738 wavelength of 550 nm (solid lines). The open circles represent all the POT-SIA particles observed during the whole
739 polluted periods at Gucheng rural and Beijing urban sites.